Chemical Science

ROYAL SOCIETY OF CHEMISTRY

EDGE ARTICLE

View Article Online
View Journal | View Issue

Cite this: *Chem. Sci.*, 2025, **16**, 23038

All publication charges for this article have been paid for by the Royal Society of Chemistry

Extended white-box cyclophanes for the synthesis of mechanically interlocked derivatives of single-walled carbon nanotubes in water

Julia Villalva,[a] Arturo Blanco-Gómez,[b] David M. Jiménez,[a] Alejandro López-Moreno,[a] M. Luisa Ruiz-González,[c] Carlos Peinador,*[b] Marcos D. García*[b] and Emilio M. Pérez*[a]

Single-walled carbon nanotubes (SWNTs) possess exceptional properties, but their inherent tendency to agglomerate has limited their exploitation. Here, we present a strategy for the aqueous synthesis of mechanically interlocked nanotube derivatives (MINTs) by combining two complementary cationic molecules that not only assist in dispersing SWNTs but also assemble around them through dynamic acyl hydrazone linkages. The resulting MINTs integrate the stability of covalent modification with the unique versatility of acyl hydrazone functionalities, enabling post-functionalization of the nanotube surface. Comprehensive characterization confirmed the successful formation of these interlocked structures, accompanied by smaller fractions of other supramolecular aggregates, while preserving the SWNT integrity. Importantly, the acyl hydrazone moieties impart intrinsic hydrolytic susceptibility, facilitating the controlled recovery of pristine nanotubes after use. This waterborne MINT platform offers a promising route for developing functional SWNT materials tailored for applications requiring both stability and reversible modification in aqueous environments.

Received 14th July 2025
Accepted 29th October 2025

DOI: 10.1039/d5sc05224f

rsc.li/chemical-science

Introduction

The fascinating host–guest properties of tetracationic bipyridinium cyclophanes have been studied since 1988, following the preparation of the renowned little blue-box by Stoddart and coworkers (**B**, Scheme 1).[1] The versatility of this molecule and analogues, and their distinctive host–guest properties have paved the way for the synthesis of a wide range of mechanically interlocked molecules, from straightforward 1 : 1 catenanes to highly intricate [5]rotaxanes.[2]

Building on Stoddart's pioneering work, numerous research groups have introduced variations of the blue-box with enhanced properties. In 2019, Peinador, García and coworkers described the preparation of a "white-box", a water-soluble self-assembled cyclophane analogue that makes use of hydrazone-based dynamic covalent chemistry for the thermodynamically controlled aqueous synthesis of cyclophane receptors.[3] This white box (**W**, Scheme 1) was prepared by acyl hydrazone bonding of complementary bis(pyridinium)xylylene tweezers in water using a template-assisted process. The ability of the white box to associate a variety of nonpolar organic guests in water, and the structural flexibility of its design, prompted us to investigate its interaction with carbon nanotubes in water.

Single-walled carbon nanotubes (SWNTs) possess unique properties, that are sometimes difficult to exploit fully with their

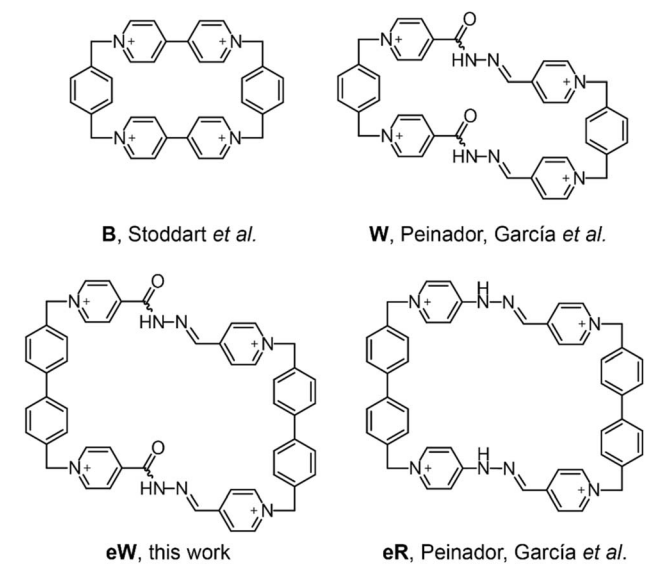

Scheme 1 Chemical structures of cyclophanes **B**, **W**, **eW** and **eR**.

[a]*IMDEA Nanociencia, C/ Faraday 9, Madrid, 28049, Spain. E-mail: emilio.perez@imdea.org*

[b]*Departamento de Química, Centro Interdisciplinar de Química e Bioloxía (CICA), Facultade de Ciencias, Universidade da Coruña, 15071, A Coruña, Spain. E-mail: carlos.peinador@udc.es; marcos.garcia1@udc.es*

[c]*Facultad de Ciencias Químicas, Departamento de Química Inorgánica, Universidad Complutense de Madrid, 28040 Madrid, Spain*

tendency to aggregate. Water is a particularly attractive solvent to disperse SWNTs, and consequently several strategies have been explored to this end, typically involving surfactant molecules that assemble around the nanotubes, enhancing their hydrophilicity. The suspension of SWNTs in water has allowed some of the most significant breakthroughs in SWNT science, including the determination of the optical bandgap of SWNTs according to their chirality,[4] the sorting of individual chiralities of SWNTs,[5] and, more recently, the separation of SWNT enantiomers.[6]

In 2014, we introduced a novel method to derivatize SWNTs as rotaxane-type mechanically interlocked derivatives (MINTs), by encapsulation of SWNTs within organic macrocycles.[7] Our method to form MINTs relied on a ring-closing metathesis reaction of alkene-terminated molecules surrounding SWNTs. We demonstrated the versatility of this method, showing that any fragment with sufficient affinity towards SWNTs could be used for MINT synthesis.[8] MINTs have proven valuable in various applications, including composite fillers,[9] catalysis[10] or molecule-based qubits.[11] Several other approaches towards MINTs have been explored, such as direct threading of SWNTs through cycloparaphenyleneacetylenes,[12] disulfide exchange,[13] or encapsulation within metallacycles.[14] All of them, however, take place in organic solvents, with the sole exception of a recent report by the von Delius group.[15]

Inspired by the binding properties of **W** in water, we hypothesized that a structurally equivalent extended cyclophane **eW** carrying two extra phenyl groups (Scheme 1), would be able to mechanically interlock SWNTs in water by means of a highly-efficient hydrazone bond-forming reaction. Experimentally, the dynamic nature of the hydrazone bond enables the formation of a diverse population of supramolecular architectures, consisting of larger macrocycles as well as higher-order oligomeric structures, suggesting that the system undergoes extensive error correction during assembly. The functionalization efficiency is enhanced by the unexpected surfactant properties of tweezer **1** (Scheme 2), which have also been investigated thoroughly.

Results and discussion

Molecule **1** was easily obtained in a single step by reacting the isonicotinichydrazide with 4,4′-bis(bromomethyl)biphenyl in refluxing acetone. This reaction yields a protected precursor as acyl hydrazone derivative, which slowly hydrolyzes in water to generate the final hydrazide **1** (molecule **1** is shown in Scheme 2a, while the hydrazone precursor is depicted in the SI, Fig. S2, as acyl hydrazone-**1**). Molecule **2** was prepared by reaction of 4-pyridinecarboxaldehyde and 4,4′-bis(bromomethyl)biphenyl in refluxing acetonitrile (see SI, S2 and S3 for the complete synthetic procedure and characterization).

In a first attempt to prepare MINTs using molecules **1** and **2**, we sonicated mixtures containing different ratios of **1**, **2** and (6,5) enriched-SWNTs (≥95% carbon basis, median length 1 μm, Sigma Aldrich). To our surprise, stable suspensions of SWNTs could be obtained when employing molecule **1**, suggesting good surfactant properties and good complementarity between the tweezer and the SWNTs.

Dispersing ability of 1

Initial dispersions were prepared by tip sonication (20% power, ice bath, 30 min) followed by centrifugation (18 626 g, 15 min) to eliminate undispersed SWNTs. Four separate (6,5)-SWNTs dispersions (0.02 wt%) were made by varying the concentration of surfactant **1** in D_2O from a 0.01 wt% (1.4×10^{-4} mM) to a 0.2 wt% (2.8×10^{-3} mM). Although higher concentrations are theoretically possible, they are not recommended due to surfactant solubility limitations. Fig. 1a shows a photograph of these four different dispersions, with no significant variations between the samples, which remained stable for several weeks.

UV-Vis-NIR absorption and PLE spectroscopies were employed to address the quality of the dispersions. The absorption spectra of the samples, shown in Fig. 1b, display the characteristic interband absorption peaks of the (6,5)-SWNT sample, alongside a background absorption likely resulting from remaining bundled nanotubes. An increase in the concentration of **1** yielded a corresponding rise in the number of suspended SWNTs, which could be quantified by integration of the interband absorption peak centred at 579 nm after accounting for background absorption (Fig. S4). A plot of the S_{22} integral against the concentration of **1** confirmed a significant 150% concentration increase in individual SWNTs when moving from a 0.01 wt% to a 0.20 wt% of **1**. For comparison, a sample containing 0.40 wt% **1** was also measured. The plateau reached at the 0.2 wt% level is attributed to **1** reaching its solubility limit.

We conducted further UV-Vis-NIR spectroscopic analyses to delve into whether **1** preferentially interacts with SWNTs of differing diameters. With our tweezer design, we envisioned perfect complementarity between **1** and the small-diameter (6,5)-SWNTs (0.78 nm wide). To test this, the dispersing properties of **1** were analysed using larger diameter SWNTs. We used a sample of mixed-chirality SWNTs, with diameters 1.6 ± 0.4 nm (Tuball, ≥99% carbon basis, length > 5 μm, OCSiAl). Experimentally, **1** was also able to disperse the large-diameter Tuball-SWNTs (grey in Fig. 1d). Further, the UV-Vis-NIR spectra of a 1 : 1 mixture comprising Tuball-SWNTs and (6,5)-SWNTs (Fig. 1d, blue line) revealed no evident selectivity towards SWNTs of a particular chirality. After background subtraction, integration of the mixture spectrum in the 500–1200 nm range matched the sum of the integration of the individual spectra of Tuball-SWNTs and (6,5)-SWNTs at equivalent concentrations (see SI, S4 for further details). We understand this result in light of the open and flexible structure of **1**, featuring two methylene groups that allow for conformational variation.

To assess the dispersion effectiveness of the hydrazide group, two alternative functional groups were tested. In the first modification, the hydrazide group was replaced by a hydrazine group, yielding molecule **3** (see SI, S2. Similar to acyl hydrazone-**1**, hydrazone-**3** slowly hydrolyzes in water to form hydrazine **3**). In the second modification, the hydrazide group was

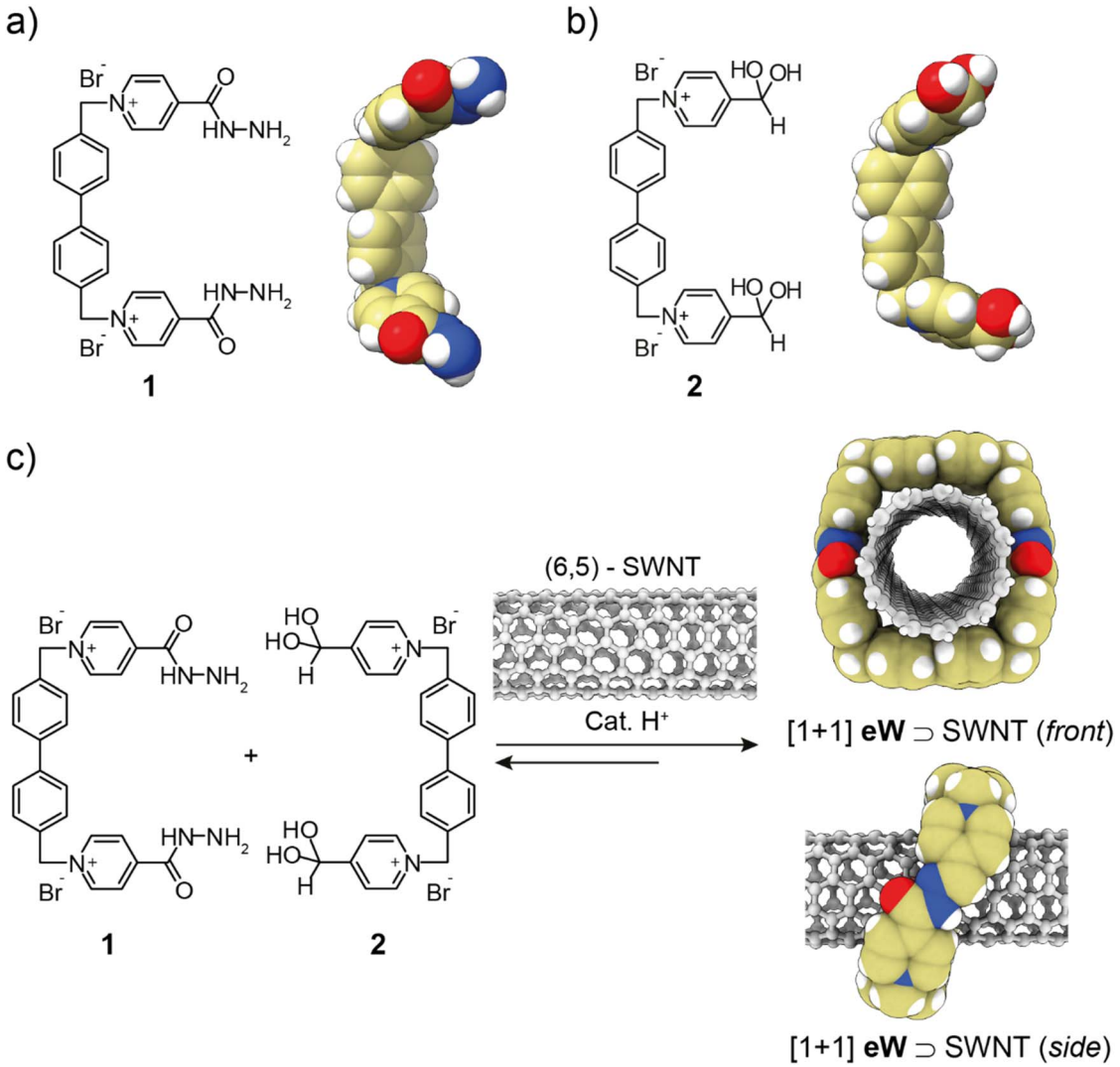

Scheme 2 (a) Chemical structure of **1** and its optimized structure; (b) chemical structure of **2** and its optimized structure; (c) reaction scheme for the preparation of acyl hydrazone MINTs (**eW**⊃SWNT) and MINT optimized structure containing the smallest [1 + 1] macrocycle. Optimizations were performed using the semiempirical GFN2-xTB tight binding method,[16] including solvation effects by means of the ALPB(water) model.[17] In **eW**⊃SWNT, C atoms from the SWNT are grey.

substituted with geminal hydroxyl groups to produce molecule **2** (Scheme 2b). Molecule **3** demonstrated some dispersing properties at equivalent concentrations (Fig. S8). Photoluminescence excitation (PLE) spectra of these dispersions showed a similar trend in photoluminescence quenching, suggesting a comparable molecular wrapping around the SWNTs (Fig. S9). In contrast, the **2** variant failed to disperse SWNTs, pointing to the combined role of pyridinium and hydrazine groups in achieving dispersion.

Although **1** exhibits lower dispersion capabilities than the widely-used surfactant sodium deoxycholate (DOC, see the SI S5 for experimental comparison), its terminal hydrazide groups offer flexibility for incorporating different hydrophobic elements, such as long alkyl chains. This property offers the possibility of developing new molecules with potentially improved surfactant features. To delve deeper into the interactions and affinities between these modified surfactants and SWNTs, we initiated the MINT synthesis experiments involving **1**, **2**, and their mixtures.

Mechanically interlocked carbon nanotubes

Our interlocking approach required mixing (6,5)-SWNTs with a 1 : 1 combination of **1** and **2** in the presence of a catalytic amount of trifluoroacetic acid (TFA). In parallel, we prepared three control samples of (6,5)-SWNT containing either **1**, **2** or a 1 : 1 mixture of both tweezers (**1** and **2**) in the absence of TFA. All mixtures were initially sonicated in H_2O for 10 minutes and then stirred overnight at 60 °C. The resulting functionalized SWNTs were washed with H_2O (3×), acetone, CH_2Cl_2 and Et_2O, following the typical procedure for MINTs synthesis (see SI, S2 for further details).[7,8,18]

Thermogravimetric analysis (Fig. 2) of the samples revealed significant differences between the products. The product formed by the mixture of (6,5)-SWNTs and a 1 : 1 combination of

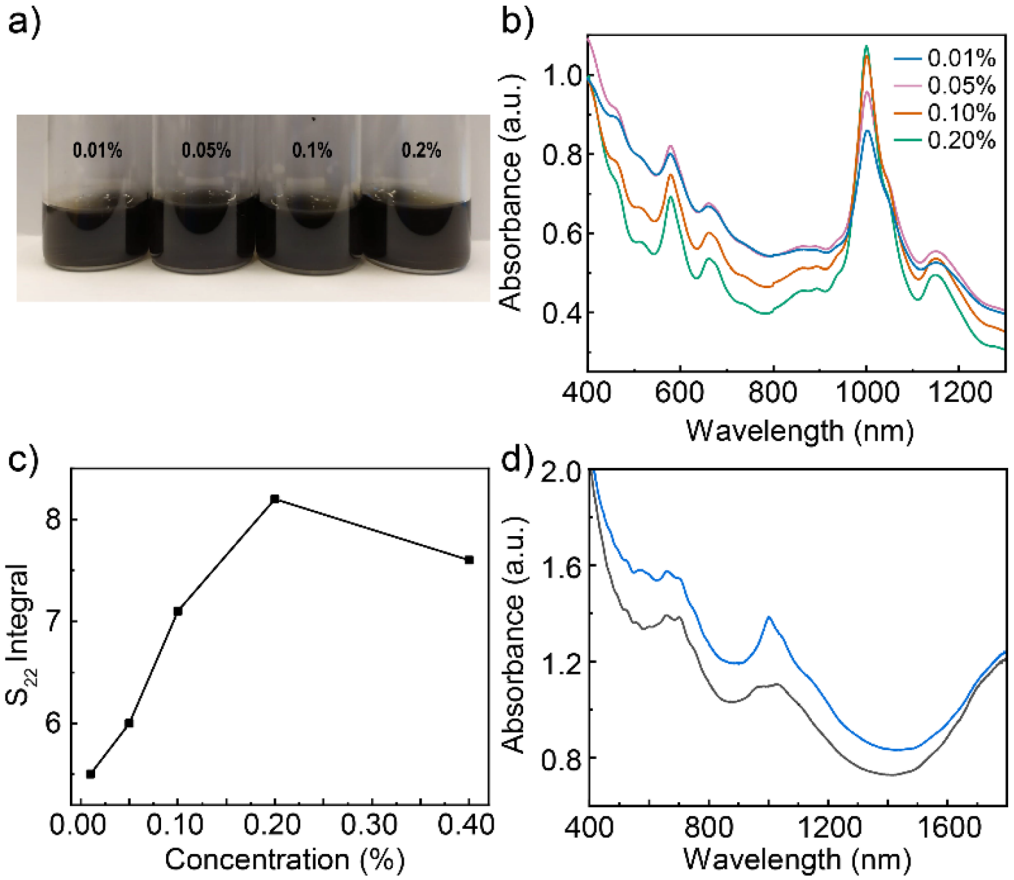

Fig. 1 (a) Photograph of the different suspensions obtained varying the percentage of tweezer **1**. The SWNT concentration is in all cases 0.02 wt%. (b) UV-Vis-NIR absorption spectra of mixtures of (6,5)-SWNTs and **1** (0.01% (blue), 0.05% (pink), 0.10% (orange) and 0.20% (green)) in D_2O. (c) Integral of the S_{22} band at 579 nm as a function of **1** concentration. The integral has been calculated after background subtraction. (d) UV-Vis-NIR absorption spectra of a mixture of Tuball-SWNTs and 0.20% **1** (0.02 wt% SWNTs in D_2O, half diluted, grey) and a mixture of 1 : 1 Tuball-SWNTs/(6,5)-SWNTs and 0.20% **1** (0.01 wt% SWNTs each sample in D_2O, blue).

1 and **2** in the presence of TFA displayed a broad weight loss process of 25% at 190–375 °C (Fig. 2a, green curve). This corresponds to approximately one **1** + **2** unit for every 300 SWNT carbon atoms. In contrast, the same mixture stirred in the absence of TFA exhibited a smaller but significant 14% weight loss (Fig. 2a, blue curve). In comparison with our results using RCM, where formation of MINTs leads to a well-defined weight loss, and the formation of oligomers leads to a separate weight loss process,[19] the TGA data suggested the TFA-catalysed formation of oligomers and/or macrocycles around the SWNTs (MINTs or **eW**⊃SWNT, from now on), while the latter implied weaker supramolecular interactions between

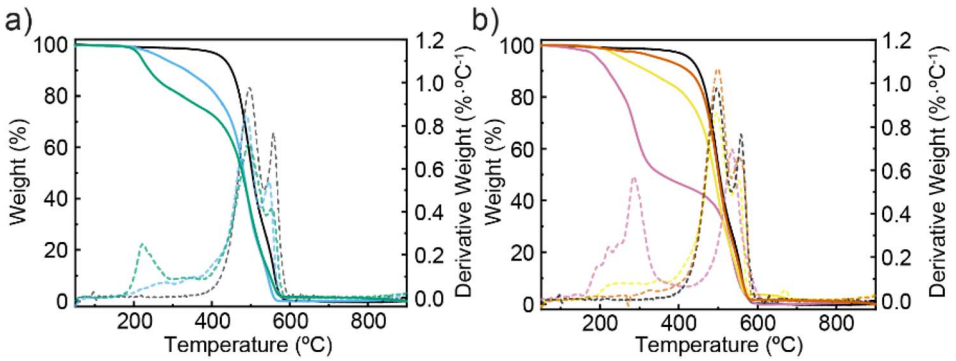

Fig. 2 (a) TGA analysis (air, 10 °C min^{-1}) of (6,5)-SWNT (black), **eW**⊃SWNT (green), and the mixture of **1** and **2** with (6,5)-SWNTs in the absence of cat. TFA (blue). (b) TGA analysis (air, 10 °C min^{-1}) of (6,5)-SWNT (black), the supramolecular complexes formed by the combination of (6,5)-SWNTs and **1** (yellow) or **2** (orange) and the equimolar mixture of **1** and **2** in absence of (6,5)-SWNTs (pink).

compounds **1** and **2** and the (6,5)-SWNTs. Analysis of the filtrates obtained during MINT preparation confirmed the presence of **1** + **2** dimers and small oligomers (Fig. S10) in the reaction catalysed by TFA. Analysis of the reaction in the absence of SWNTs (Fig. S11) provided similar results, confirming that large oligomers or macrocycles are not obtained in significant proportions under our reaction conditions. Further scrutiny of the thermogravimetric profile of the final compounds revealed that the supramolecular adsorption of **1** was associated with a 15% reduction in sample weight (Fig. 2b, yellow curve). In contrast, the adsorption of **2** was markedly less robust, constituting a mere 6% of the final sample mass (Fig. 2b, orange curve). These results are in agreement with the ability of **1** to disperse SWNTs as described above.

To further investigate the structure of the different (6,5)-SWNT derivatives, their absorption and emission spectra were acquired after dispersion in D_2O employing 1 wt% DOC (Fig. 3). The normalized SWNT emission intensities at λ_{exc} = 565 nm demonstrated a discernible attenuation in photoluminescence attributable to binding effects. This photoluminescence quenching was markedly pronounced in the **eW**⊃SWNT sample – exhibiting a 54% reduction in luminescence –, and in the sample with adsorbed **1**, displaying a 42% reduction. These outcomes contrasted with those from the 1 : 1 mixture of **1** and **2** with SWNTs in the absence of TFA, which only showed a 22% quench in luminescence intensity, and the sample with adsorbed **2**, which exhibited an 11% quench.

The heightened quenching in the cases of **eW**⊃SWNT formation and **1** adsorption can be attributed to a more extensive coverage of organic material on the SWNTs, thereby affecting the photoluminescence properties of the SWNTs. The quenching of photoluminescence is a direct indication of intimate macrocycle–SWNT interaction which we often find in MINT formation.[7,10a,c,13,14,18a]

To investigate the possibility of supramolecular adsorption of macrocycles during the MINT-forming reaction, an additional control sample consisting of a mixture of (6,5)-SWNTs with pre-synthesized **eW** was prepared under the same conditions described above. As shown in Fig. 4, TGA revealed an 11% weight loss at 190–375 °C. This weight loss is sufficiently different from the **eW**⊃SWNT sample (25%), effectively proving the role of hydrazone bond formation in the presence of SWNTs and TFA.

Next, the stability of the acyl hydrazone derivatives in **eW**⊃SWNT was evaluated. The samples were subjected to two sequential hot water washes at 100 °C for 1 hour each, followed by filtration. To ensure reproducibility, each of these experiments was repeated three times. TGA was conducted after each wash to monitor the weight loss at 375 °C. The average weight loss attributed to the macrocycle decomposition was reduced from a 22% to a 9% after the first wash, as expected due to the hydrolysis susceptibility of the acyl hydrazone groups under elevated temperatures. A second hot wash did not reduce further the macrocycle content, indicating complete hydrolysis during the first wash, with the residual weight loss being comparable to that found when using just **1**.

To explore this further, the acyl hydrazone functionalities in **eW**⊃SWNT were locked by reduction with sodium borohydride to the corresponding hydrazide, which cannot be hydrolyzed. As expected, these modified derivatives demonstrated significant stability when subjected to two sequential hot washes (Fig. 4b, orange). Alternatively, increased stability was also achieved by removing the acyl groups from the acyl hydrazone. A final MINT sample (**eR**⊃SWNT), consisting of **eR** macrocycles (Scheme 1, extended redbox recently published by some of us[20]), was prepared following the standard procedure using a mixture of (6,5)-SWNTs and tweezers **2** and **3** (see SI, S2 for chemical structure). This sample showed increased resistance to hydrolysis, losing only a minimal fraction of its weight during each acid wash (Fig. 4b, blue). The **eR**⊃SWNT functionalization yields were comparable to those obtained with the original acyl hydrazone macrocycles, indicating that improved stability can be achieved without compromising functionalization efficacy. While these results are encouraging, the characterization of the **eR**⊃SWNT derivatives is still limited, and further studies will be necessary to fully evaluate their properties and stability.

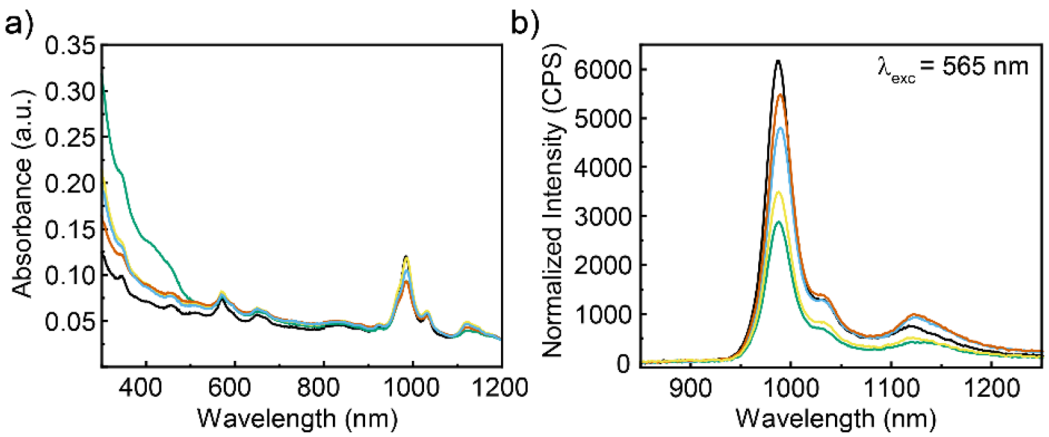

Fig. 3 (a) UV-Vis-NIR spectra (D_2O (DOC, 1 wt%)) of (6,5)-SWNT (black), **eW**⊃SWNT (green), the mixture of **1** and **2** with (6,5)-SWNTs in the absence of cat. TFA (blue), the supramolecular complex formed by stirring **1** and (6,5)-SWNTs (yellow) and the supramolecular complex formed by stirring **2** and SWNTs (orange). (b) Normalized photoluminescence emission spectra with λ_{exc} = 565 nm for the samples indicated in (a).

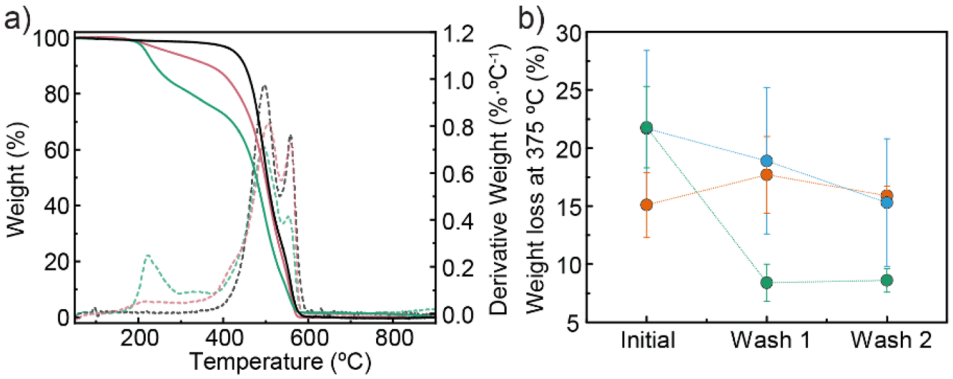

Fig. 4 (a) TGA analysis (air, 10 °C min^{-1}) of (6,5)-SWNT (black), **eW**⊃SWNT (green) and the supramolecular mixture of (6,5)-SWNTs with **eW** (pink). (b) TGA weight losses at 375 °C (air, 10 °C min^{-1}) before and after two hot washes in **eW**⊃SWNT (green), **eW**⊃SWNT submitted to $NaBH_4$ treatment (orange) and **eR**⊃SWNT (blue).

Considering the high acidity of TFA, a thorough Raman spectroscopy analysis was conducted on the **eW**⊃SWNT sample and the supramolecular control consisting of a mixture of **1** and **2** with (6,5)-SWNTs in the absence of TFA, to investigate the possible introduction of defects during formation of **eW**⊃SWNT. Upon 532 nm excitation (Fig. S12a), no notable differences were observed between the Raman spectra of **eW**⊃SWNT, the supramolecular control and the pristine (6,5)-SWNTs. Most importantly, there was no significant increase in the relative intensity of the D band, proving that the covalent structure of the SWNT remains intact after the formation of **eW**⊃SWNT. Additionally, RBM and G bands (Fig. S12b and c) displayed similar behaviour among the samples. The 2D *vs.* G Raman shift maps (Fig. S12d) further revealed a comparable

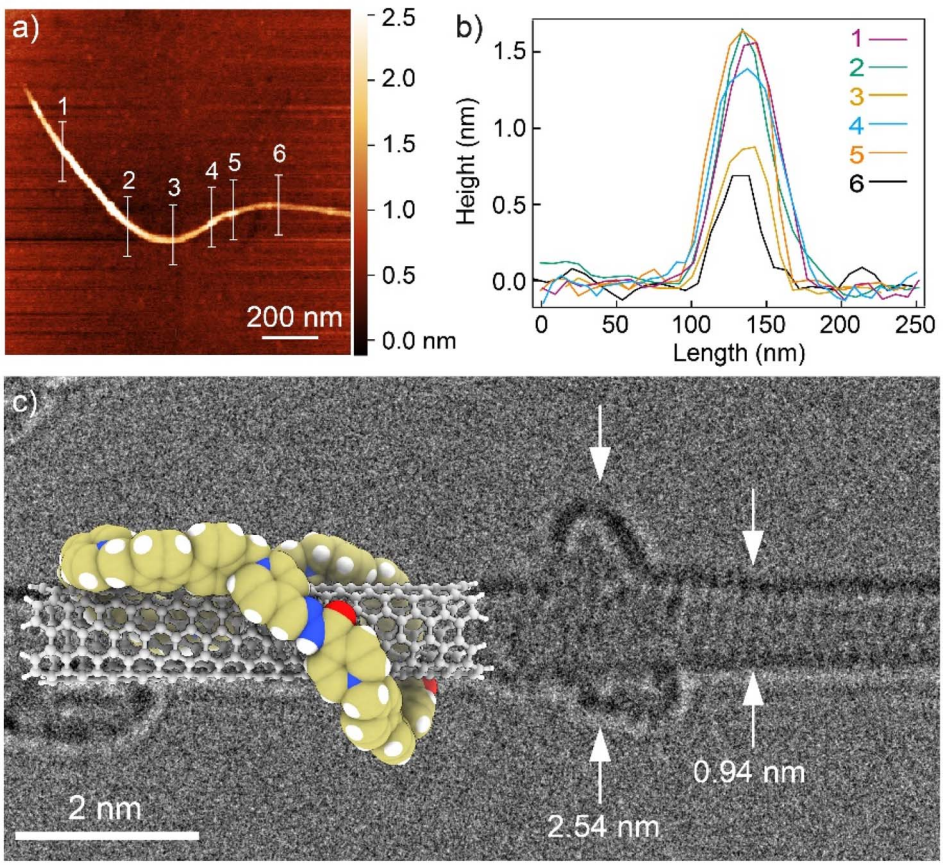

Fig. 5 (a) AFM topographic image of a **eW**⊃SWNT suspension in iPrOH and (b) height profiles along the lines marked in (a). (c) AC-HRTEM image of a SWNT containing a macrocycle (acceleration voltage 60 kV) and [2 + 2] **eW**⊃SWNT optimized structure.

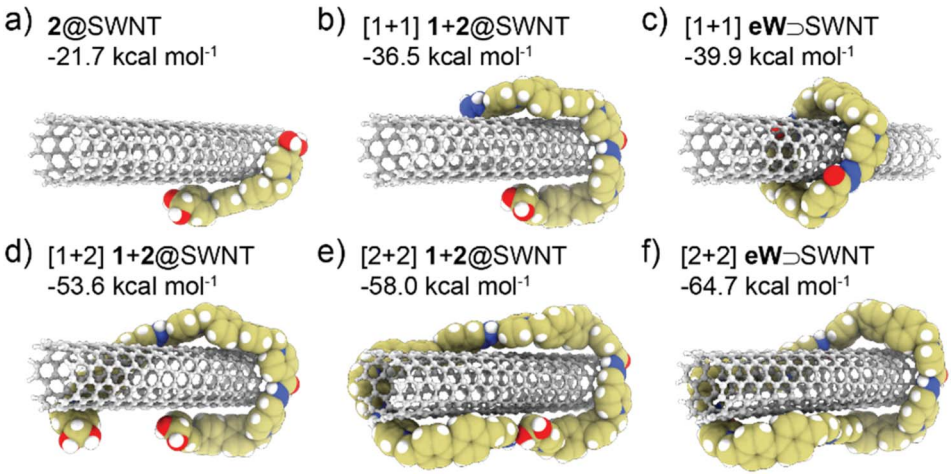

Fig. 6 Local minima and ΔG_a° values in kcal mol^{-1} computed at the ωB97X-3c/SMD(H_2O)//GFN2/ALPB(H_2O) level of theory,[16,17,22,23] for the potential aggregates formed by the association between a truncated hydrogen-capped section of a (6,5)-SWNT (ball-and-stick), and cyclic (c and f)/oligomeric (a, b, d and e) species arisen from the self-assembly of building blocks **1** and **2** (van der Waals spheres).

trend among the three samples, indicating negligible SWNT doping upon strapping with **eW**.

Microscopic AFM and TEM analysis provided results consistent with the formation of MINTs. Fig. 5a and b present an AFM micrograph consisting of a single **eW**⊃SWNT and its corresponding height profiles. The individualized SWNT shown, with a height of approximately 0.8 nm, exhibits several elevations ranging from about 1.4 nm to 1.6 nm. The left section of the SWNTs shows a dense accumulation of organic material with an elevation of around 1.5 nm, consistent with the high functionalization observed for **eW**⊃SWNT. Aberration-corrected HR-TEM analysis (60 kV) of **eW**⊃SWNT shows mostly bundled nanotubes with heavily functionalized sidewalls (SI, S13), in agreement with the TGA data. In some instances, like in Fig. 5c and S14, we can observe individual macrocycles around the SWNT (the calculated macrocycle [2 + 2] **eW**⊃SWNT is superimposed for comparison). For a statistically significant analysis of the microscopic characterization, we determined the spacing between adjacent nanotubes within bundles. Because most tubes remain in van der Waals contact ($d = 0$), these measurements effectively represent the smallest possible intertube separations. For **eW**⊃SWNT, the average distance of 0.11 ± 0.04 nm ($N = 50$) is approximately twice that observed in pristine SWNT bundles (0.06 ± 0.06 nm, $N = 50$). This increase in spacing indicates a de-bundling effect driven by extensive functionalization, in agreement with our prior observations.[21]

To shed some light on the differences in binding strength between (6,5)-SWNTs and the potential species produced during the self-assembly of **1** and **2**, the standard Gibbs free energy of association (ΔG_a°) in aqueous media at 298.15 K was computed using a multilevel approach based on state-of-the-art electronic structure methods.[22] A simplified reaction was modelled involving a hydrogen-capped section of a (6,5)-SWNT approximately 4 nm in length (509 atoms), small enough to be computationally tractable yet large enough to capture interactions with either the hydrazide/diol building blocks or the resulting cyclic/oligomeric species formed *via* acyl hydrazone bonding of up to four monomers. As shown in Fig. 6 and Tables S1 and S2, the data support exergonic association processes for all considered species, but with both cyclic and linear oligomerization processes becoming increasingly favored as the number of acyl hydrazone-linked monomers increases. Our calculations are in line with the experimental findings, in that there are no major energetic differences per cyclophane unit between the interlocked species and the supramolecular association of oligomers, supporting the coexistence of both under thermodynamic equilibrium. Moreover, we observe that the [2 + 2] **eW**⊃SWNT structure, observed experimentally under AC-HRTEM (Fig. 5), is particularly stable, with $\Delta G_a^\circ = -64.7$ kcal mol^{-1}.

Conclusion

We have synthesized two novel surfactants that individually displayed modest to negligible dispersing ability compared to established surfactants like DOC. While their surfactability is limited, the versatile hydrazone functionalities offer promising avenues for future activity optimization. By combining molecules **1** and **2**, we first utilised surfactants as recognition motifs to construct MINTs in water. The assembly of these MINTs was rigorously confirmed through thermogravimetric analysis, combined with spectroscopic and microscopic techniques. These analyses validated the formation of MINTs and demonstrably preserved the integrity of the encapsulated nanotubes. In this case, as opposed to our previous reports using RCM, in the final products MINTs are accompanied by other supramolecular aggregates, at least to some extent. In line with this, semiempirical calculations show that there are no major differences in stability per cyclophane unit between the interlocked species and the supramolecularly associated oligomers, although some species, like the interlocked [2 + 2] **eW**⊃SWNT

observed experimentally under AC-HRTEM, seem particularly stable. Notably, these water-borne MINTs possess inherent hydrolytic susceptibility, enabling the post-functionalization retrieval of intact nanotubes. Compared to previous examples restricted to organic media, these novel MINTs hold significant promise for applications requiring aqueous environments. Recently-reported work by some of the authors has demonstrated the easy *exo*-functionalization of **eW** analogues with hydrazide pendants,[24] results that open the door for the expansion of the self-assembly strategy reported herein for the introduction of further functionalization into this type of MINTs.

Author contributions

The manuscript was written through contributions of all authors. All authors have given approval to the final version of the manuscript.

Conflicts of interest

There are no conflicts to declare.

Data availability

All data are available within the manuscript, supplementary information (SI) and **https://www.nanociencia.imdea.org/services/repository**.

Supplementary information: general methods and materials, synthetic and characterization data for compound **1** and mechanically interlocked SWNTs, additional UV-Vis and PLE spectra, Raman analysis, additional HRTEM micrographs and computational details. See DOI: **https://doi.org/10.1039/d5sc05224f**.

Acknowledgements

We gratefully acknowledge financial support from the Ministry of Science of Spain (PID2020-116661RB-I00; MCIN/AEI/10.13039/501100011033; PID2022-137361NB-I00; PID2023-152267NB-I00), Comunidad de Madrid (MAD2D-CM)-IMDEA project funded by Comunidad de Madrid, by the Recovery, Transformation and Resilience Plan, and by NextGenerationEU from the European Union, and the Consellería de Cultura, Educación e Universidade da Xunta de Galicia (ED431C 2022/39). IMDEA Nanociencia received support from the "Severo Ochoa" Programme for Centres of Excellence in R&D (MINECO, Grant CEX2020-001039-S). A. B.-G. thanks the Consellería de Cultura, Educación e Universidade da Xunta de Galicia for his postdoctoral fellowships (ED481D-2024-020). We acknowledge CESGA (Xunta de Galicia) for computational time. Funding for open access charge: Universidade da Coruña/CISUG.

References

1 X.-Y. Chen, H. Chen and J. F. Stoddart, *Angew. Chem., Int. Ed.*, 2023, **62**, e202211387.
2 E. J. Dale, N. A. Vermeulen, M. Juríček, J. C. Barnes, R. M. Young, M. R. Wasielewski and J. F. Stoddart, *Acc. Chem. Res.*, 2016, **49**, 262–273.
3 (*a*) A. Blanco-Gómez, Á. Fernández-Blanco, V. Blanco, J. Rodríguez, C. Peinador and M. D. García, *J. Am. Chem. Soc.*, 2019, **141**, 3959–3964; (*b*) A. Blanco-Gómez, I. Neira, J. L. Barriada, M. Melle-Franco, C. Peinador and M. D. García, *Chem. Sci.*, 2019, **10**, 10680–10686; (*c*) P. Cortón, H. Wang, I. Neira, A. Blanco-Gómez, E. Pazos, C. Peinador, H. Li and M. D. García, *Org. Chem. Front.*, 2022, **9**, 81–87; (*d*) I. Neira, A. Blanco-Gómez, J. M. Quintela, M. D. García and C. Peinador, *Acc. Chem. Res.*, 2020, **53**, 2336–2346.
4 S. M. Bachilo, M. S. Strano, C. Kittrell, R. H. Hauge, R. E. Smalley and R. B. Weisman, *Science*, 2002, **298**, 2361–2366.
5 X. Tu, S. Manohar, A. Jagota and M. Zheng, *Nature*, 2009, **460**, 250–253.
6 H. Li, C. M. Sims, R. Kang, F. Biedermann, J. A. Fagan and B. S. Flavel, *Carbon*, 2023, **204**, 475–483.
7 A. de Juan, Y. Pouillon, L. Ruiz-González, A. Torres-Pardo, S. Casado, N. Martín, Á. Rubio and E. M. Pérez, *Angew. Chem., Int. Ed.*, 2014, **53**, 5394–5400.
8 A. Lopez-Moreno and E. M. Perez, *Chem. Commun.*, 2015, **51**, 5421–5424.
9 (*a*) A. Lopez-Moreno, B. Nieto-Ortega, M. Moffa, A. de Juan, M. M. Bernal, J. P. Fernandez-Blazquez, J. J. Vilatela, D. Pisignano and E. M. Perez, *ACS Nano*, 2016, **10**, 8012–8018; (*b*) S. Mena-Hernando, M. Eaton, J. P. Fernández-Blázquez, A. López-Moreno, H. Pedersen and E. M. Pérez, *Chem.–Eur. J.*, 2023, **29**, e202301490; (*c*) J. Villalva, A. Rapakousiou, M. A. Monclús, J. P. Fernández Blázquez, J. de la Vega, A. Naranjo, M. Vera-Hidalgo, M. L. Ruiz-González, H. Pedersen and E. M. Pérez, *ACS Nano*, 2023, **17**, 16565–16572; (*d*) M. Lundorf, H. Pedersen and T. Dehli, *US Pat.*, 11028240, 2015; (*e*) H. Pedersen, M. D. Lundorf and C. B. O. Nielsen, *EP Pat.*, 3737711, 2018; (*f*) A. Rapakousiou, E. M. Pérez, H. Pedersen, M. D. Lundorf and J. Villalva, *PCT Pat.*, WO2022/067741, 2021; (*g*) H. S. Mena, E. M. Pérez, W. Xu, W. Zhang, H. Pedersen, M. D. Lundorf and A. López-Moreno, *PCT Pat.*, WO2022/067756, 2021; (*h*) H. Pedersen, M. González, A. López-Moreno, J. Villalva Fernández, M. d. L. Gonzalez-Juarez, M. Eaton, D. Pérez, M. D. Lundorf, *et al.*, *PCT Pat.*, WO2022/067728, 2021; (*i*) J. Villalva, H. Pedersen, A. López-Moreno, M. González, E. M. Pérez, J. González, M. d. L. Lourdes, M. Rivas-Caramés, M. D. Eaton, I. Isasti, *et al.*, *EP Pat.*, 22382606.6, 2022; (*j*) M. González-Sánchez, H. Pedersen, A. López-Moreno, J. Villalva, M. D. Eaton, M. d. L. González-Juárez, E. M. Pérez, I. Isasti, S. Miranda-Alcázar, M. Rivas-Caramés, *et al.*, *EP Pat.*, 23382038.0, 2022.
10 (*a*) M. Blanco, B. Nieto-Ortega, A. de Juan, M. Vera-Hidalgo, A. López-Moreno, S. Casado, L. R. González, H. Sawada, J. M. González-Calbet and E. M. Pérez, *Nat. Commun.*, 2018, **9**, 2671; (*b*) D. Wielend, M. Vera-Hidalgo, H. Seelajaroen, N. S. Sariciftci, E. M. Pérez and D. R. Whang, *ACS Appl. Mater. Interfaces*, 2020, **12**, 32615–

32621; (*c*) W. Zhang, M. Guillén-Soler, S. Moreno-Da Silva, A. López-Moreno, L. R. González, M. d. C. Giménez-López and E. M. Pérez, *Chem. Sci.*, 2022, **13**, 9706–9712.

11 S. Moreno-Da Silva, J. I. Martínez, A. Develioglu, B. Nieto-Ortega, L. de Juan-Fernández, L. Ruiz-Gonzalez, A. Picón, S. Oberli, P. J. Alonso, D. Moonshiram, *et al.*, *J. Am. Chem. Soc.*, 2021, **143**, 21286–21293.

12 K. Miki, K. Saiki, T. Umeyama, J. Baek, T. Noda, H. Imahori, Y. Sato, K. Suenaga and K. Ohe, *Small*, 2018, **14**, 1800720.

13 B. Balakrishna, A. Menon, K. Cao, S. Gsänger, S. B. Beil, J. Villalva, O. Shyshov, O. Martin, A. Hirsch, B. Meyer, *et al.*, *Angew. Chem., Int. Ed.*, 2020, **59**, 18774–18785.

14 A. López-Moreno, S. Ibáñez, S. Moreno-Da Silva, L. Ruiz-González, N. M. Sabanés, E. Peris and E. M. Pérez, *Angew. Chem., Int. Ed.*, 2022, **61**, e202208189.

15 J. Kraus, L. Meingast, J. Hald, S. B. Beil, J. Biskupek, C. L. Ritterhoff, S. Gsänger, J. Eisenkolb, B. Meyer, U. Kaiser, *et al.*, *Angew. Chem., Int. Ed.*, 2024, **63**, e202402417.

16 C. Bannwarth, S. Ehlert and S. Grimme, *J. Chem. Theory Comput.*, 2019, **15**, 1652–1671.

17 S. Ehlert, M. Stahn, S. Spicher and S. Grimme, *J. Chem. Theory Comput.*, 2021, **17**, 4250–4261.

18 (*a*) L. de Juan-Fernández, P. W. Münich, A. Puthiyedath, B. Nieto-Ortega, S. Casado, L. Ruiz-González, E. M. Pérez and D. M. Guldi, *Chem. Sci.*, 2018, **9**, 6779–6784; (*b*) S. Leret, Y. Pouillon, S. Casado, C. Navio, A. Rubio and E. M. Perez, *Chem. Sci.*, 2017, **8**, 1927–1935.

19 A. de Juan, M. Mar Bernal and E. M. Perez, *ChemPlusChem*, 2015, **80**, 1153–1157.

20 N. Fernández-Labandeira, I. Montes de Oca, E. Pazos, A. Blanco-Gómez, C. Peinador and M. D. García, *J. Org. Chem.*, 2025, **90**, 8621–8627.

21 A. Naranjo, D. M. Jiménez, M. Rivas-Caramés, J. Villalva, M. L. Ruiz-González, H. Pedersen, A. López-Moreno and E. M. Pérez, *Chem.–Eur. J.*, 2025, **31**, e202404762.

22 M. Bursch, J.-M. Mewes, A. Hansen and S. Grimme, *Angew. Chem., Int. Ed.*, 2022, **61**, e202205735.

23 (*a*) M. Müller, A. Hansen and S. Grimme, *J. Chem. Phys.*, 2023, **158**, 014103; (*b*) A. V. Marenich, C. J. Cramer and D. G. Truhlar, *J. Phys. Chem. B*, 2009, **113**, 6378–6396.

24 P. Cortón, N. Fernández-Labandeira, M. Díaz-Abellás, C. Peinador, E. Pazos, A. Blanco-Gómez and M. D. García, *J. Org. Chem.*, 2023, **88**, 6784–6790.